Carbazole Isomerism in Helical Radical Cations: Spin Delocalization and SOMO–HOMO Level Inversion in the Diradical State

Sitthichok Kasemthaveechok, Laura Abella, Marion Jean, Marie Cordier, Nicolas Vanthuyne, Thierry Guizouarn, Olivier Cador, Jochen Autschbach, Jeanne Crassous, Ludovic Favereau

Carbazole Isomerism in Helical Radical Cations: Spin Delocalization and SOMO-HOMO Level Inversion in the Diradical State

Sitthichok Kasemthaveechok,[†] Laura Abella,[‡] Marion Jean,[§] Marie Cordier,[†] Nicolas Vanthuyne,[§] Thierry Guizouarn,[†] Olivier Cador,[†] Jochen Autschbach,*[,‡] Jeanne Crassous,[†] and Ludovic Favereau,*[,†]

[†] Univ Rennes, CNRS, ISCR - UMR 6226, F-35000 Rennes, France.
[‡] Department of Chemistry, University at Buffalo, State University of New York, Buffalo, New York 14260, USA.
[§] Aix Marseille University, CNRS Centrale Marseille, iSm2, 13284 Marseille, France.

ABSTRACT: We report a new molecular design to afford persistent chiral organic open-shell systems with configurational stabilities and an inversion in energy of the singly occupied molecular orbital (SOMO) and the highest doubly occupied molecular orbital (HOMO) for both mono- and diradical states. We discovered that the unpaired electron(s) delocalization within the designed extended helical π-conjugated systems is a crucial factor to reach chemical stabilities, which is not obtained using the classical steric protection approach. The unique features of the obtained helical monoradicals allow us to explore chiral intramolecular electron transfer (IET) process in solvents of different polarity by means of optical and chiroptical spectroscopies, resulting in an unprecedented electronic circular dichroism (ECD) sign inversion for the radical transitions. We also characterized in depth the corresponding helical diradicals, which show near infrared electronic circular dichroism up to 1100 nm and an antiferromagnetic coupling between the spins, with an estimated singlet-triplet gap (ΔE_{ST}) in the range of -1.3 kcal mol^{-1}. Interestingly, our findings also revealed an intriguing double SOMO-HOMO inversion (SHI) electronic configuration for these diradicals, affording new fundamental insights regarding the peculiar ordering of electron within radicals' orbitals, and its impact on the corresponding (chiral) optoelectronic properties.

INTRODUCTION

Organic open-shell molecules continue to attract significant interest in chemistry and biochemistry due to their specific (photo-)reactivity, playing notably a central role in many enzymatic reactions, as well as in *in-vivo* imaging.[1-3] In materials science, organic radicals have also become a topic of intense research rendering them innovative alternatives for the basis of next-generation optoelectronics such as in organic field-effect transistors (OFETs), organic light-emitting diodes (OLEDs), or for organic magnets. [4-26] Recently, research in this area has started to focus on a specific class of open-shell systems, showing an energetic inversion of the singly occupied molecular orbital (SOMO) and the highest doubly occupied molecular orbital (HOMO) level (Figure 1).[27-31] SOMO-HOMO inversion (SHI) has been investigated in organic spin-polarized donor systems to afford high-spin diradicals,[16, 32-36] and also in the case of luminescent radicals in which SHI has been associated with increased photostability.[37] Organic SHI radicals have therefore generated widespread interest, both theoretically and experimentally, to rationalize and understand the consequences of the peculiar orbital energetics of this particular class of open-shell systems. [21, 29-30, 38-40] Recently, some of us put forward the first explanation why SHI appears in the first place, along with molecular design strategies for new SHI radicals.[41]

Merging the attractive properties of an organic radical within a chiral π-conjugated system has also been pursued to exploit near-infrared (NIR) circularly polarized (CP) light absorption,[29, 31, 42-52] radical CP luminescence (CPL),[53-54] and possibly enhanced spin-filtering properties,[55] as additional features in optoelectronic applications. [56-57 58 59] However, the design of stable intrinsically chiral radicals[60] remains a considerable scientific challenge due to the dual problematics of chemical reactivity and poor configurational stability.[61] As a result, few examples of persistent chiral open-shell organic radicals have been reported, which currently hampers a complete understanding of the structural and electronic factors resulting from the molecular union of chirality and spin. Beyond monoradicals, diradicals are even much more difficult to obtain due to the difficulty to stabilize two unpaired electrons within the same chiral molecular system (Figure 1).

We recently contributed to this research area by developing the first enantiopure chiral monoradical with SHI (Figure 1a).[62] Interestingly, our findings revealed that such electronic configuration contributes to stabilize unprotected chiral carbazole monoradical, while providing upon oxidation, an interesting approach for isolating one of the rare persistent organic chiral diradicals.[31, 46] Our results also showed that SHI is not a sufficient prerequisite to promote radical stability, as also recently illustrated by Rajca *et al.*.[63] Indeed, helical bicarbazole monoradical **1**$^{\bullet+}$ (Figure 1b) remains highly reactive despite SHI and the use of steric *t*-Bu groups (**1a**$^{\bullet+}$), in contrast to its axial counterpart. While this difference has been explained in terms of electronic coupling between the SOMO and HOMO levels, it appears crucial to further understand how and why such subtitle structural factor lead to a dramatic change of stability. Accordingly, further electronic and steric arguments need to be investigated to fully take advantage of SHI in chiral molecular materials and propose new design strategies for developing innovative chiral diradicals with potentially high-spin (triplet) ground state.[31]

To address this objective, we report herein the synthesis of innovative helical organic tetracarbazole systems **2** and **3** (Figure

1b), that are able to form persistent and configurationally stable mono- and diradicals. Experimental and theoretical investigations of their photophysical, chiroptical and electrochemical properties revealed that both monoradicals show SHI, configurational stability, with half-lifes up to 3 days in solution at room temperature. This persistency allowed us to study the impact of solvent polarity on the chiroptical properties of these radicals, revealing unprecedented electronic circular dichroism (ECD) sign inversion of the radical absorption transitions. Beyond these innovative findings, further oxidation of these compounds affords innovative helical diradicals which show chemical and configurational stabilities, with an unexpected SHI and nearly degenerate singlet-triplet ground states.

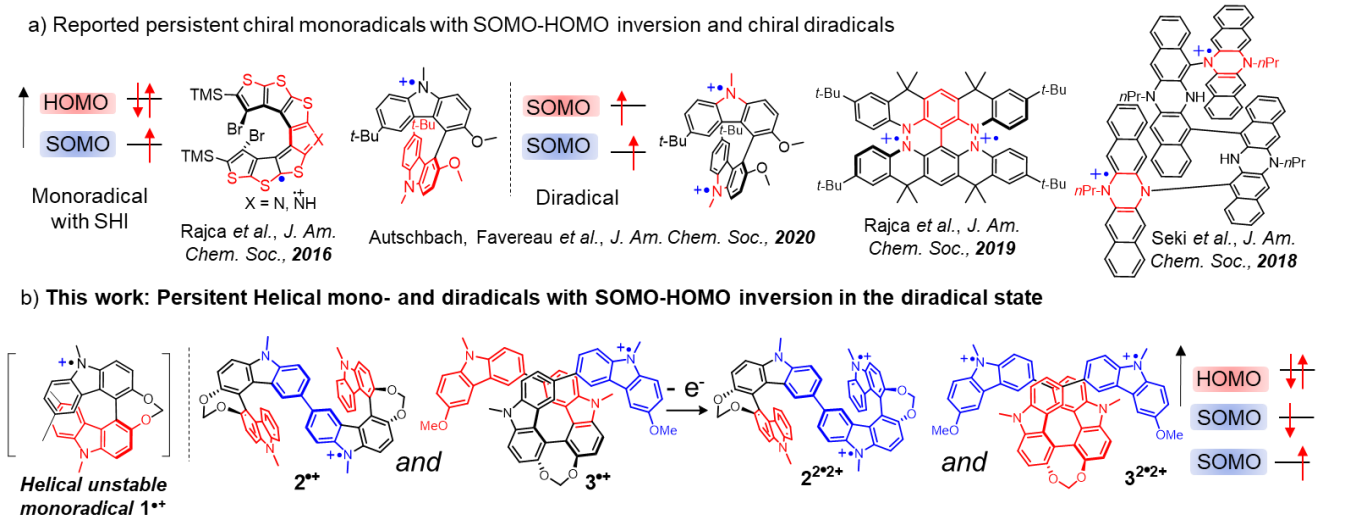

Figure 1. a) Left: examples of reported persistent chiral SHI monoradicals (note that only the racemic version of the aza-thia[7]helicene radical was reported by Rajca *et al*). The molecular fragment on which the HOMO is predominantly localized is highlighted in red, the SOMO in blue; Right: currently reported persistent chiral diradicals; b) Novel helically mono- and diradicals cationic carbazole derivatives obtained in this work, with a schematic illustration of the SHI present in both mono- and diradical derivatives (counter-ions are omitted for clarity reasons).

RESULTS AND DISCUSSION

Synthesis and Structural characterizations. We first prepared tetracarbazole derivatives **2** and **3** from their common precursor **1** (Scheme 1). (+)- and (-)-**2** were quantitatively obtained from an oxidative homocoupling reaction of enantiopure (+)- and (-)-**1**, respectively, using trifluoroacetic acid and 2,3-dichloro-5,6-dicyano-1,4-benzoquinone, DDQ, as a chemical oxidant.[64] The synthesis of **3** firstly involved the iodination of **1** at the 6 and 6' positions of both carbazole units,[65] followed by a Suzuki coupling reaction with 6-pinacoloboro-3-methoxy-9-methyl-9H-carbazole, in an overall 15% yield. Corresponding (+) and (-)-**3** enantiomers were finally obtained through chiral HPLC (see ESI for details). Model compound **4** was obtained using a similar methodology in an overall 50% yield, since the direct oxidative homocoupling of 3-methoxy-9-methyl-9H-carbazole, **CBzOMe** (Scheme 1), provided a complex mixture of homocoupling carbazole units at different positions.

X-Ray structures analyses confirmed the obtained structures for (-)-**2** and *rac*-**3**, which crystallized in the P_{21} and P_{-1} space groups, respectively. Similar dihedral angles of 52-53° were determined for the 4,4'-bicarbazole fragment of **2** and **3** (θ_a, Scheme 1), a value close to the ones measured for helical bicarbazole **1** and carbo[6]helicene.[62, 66-68] In contrast, the 6,6'-bicarbazole connection adopts an opposite arrangement between **2** and **3**, with a typical *trans* configuration for the former while for the latter, the two carbazole units of each branch are pointing outwards, forming a π-extended molecular helix. Corresponding torsion angles are also different, with values of 32.3° and 47.5° for **2** and **3**, respectively (θ_b, Scheme 1b & c). Several CH-π interactions can be identified between protons of the inner carbazole units and the aromatic rings of the peripheral carbazole fragments, as depicted in Scheme 1b & c for H^5 and H^7 of **2**, and for H^5 and $H^{5'}$ of **3** (H-centroid distances between of 2.933 and 3.285 Å). These interactions seem to be also present in solution as evidenced by the highly shielded ^{1}H NMR aromatic signals found at 5 - 6 ppm for these protons, in comparison to the model bicarbazoles **1** and **4**, respectively (Figure S1). Moreover, the 1,3-dioxepine protons of **2** show an AB quartet system in the ^{1}H NMR spectrum instead of a sharp singlet signal as for **1** and **3**, indicating a difference between the two protons' environments, and therefore a more rigid system. The full experimental conditions and characterizations (NMR and mass spectrometry) of all compounds are detailed in the ESI. Density functional theory (DFT) calculations confirmed the obtained structure for **3** while for **2**, two conformers were found, which differ by the configuration at the 6,6'-bicarbazole connection. In fact, it seems that **2** does not crystallize in its lowest-energy conformer due to crystal packing since the most stable conformer in energy by 3.6 kcal·mol^{-1} appears to be the one having a similar 6,6'bicarbazole connection than for **3** (see ESI for further information).

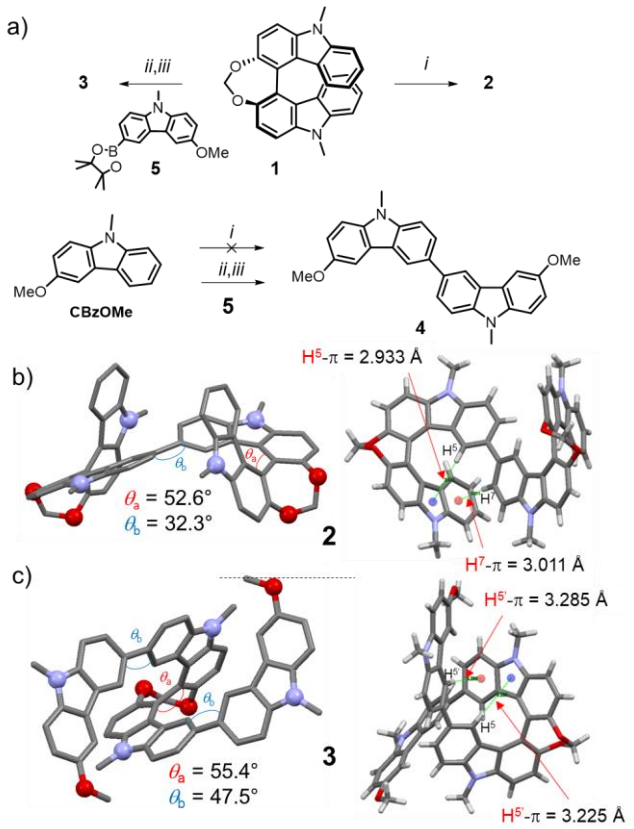

Scheme 1. a) Schematic synthetic route for **2**, **3** and **4**. Reaction conditions: *i*) DDQ, trifluoroacetic acid, CH_2Cl_2, rt, quantitative; *ii*) *N*-iodosuccinimide, AcOH, $CHCl_3$, rt. (*iii*) $Pd(PPh_3)_4$, K_2CO_3, DMF, H_2O, Ar, 110˚C, 19% and 50% yield for **3** and **4**, respectively (over two steps). X-ray structures of **2** (b) and **3** (c) with different views and the dihedral angles between the carbazole units, and the CH-π interactions present within the structures (hydrogen atoms are omitted for clarity reasons in some drawings).

Computational Details. Kohn-Sham density functional theory (DFT) as implemented in the Gaussian (G16) package was used for all computations,[69] employing the PBE0 functional[70] and the def2-SV(P) basis.[71-72] For neutral and oxidized species, solvent effects were considered by means of the polarizable continuum model (PCM) for dichloromethane and acetonitrile,[73] respectively, to match the experimental conditions. 'D3' dispersion corrections were included in the calculations.[74] For open-shell systems, i.e., radicals, the calculations were of the spin-unrestricted flavor (UDFT) except where noted in the SI. Excited state energies, transition moments, excited state structures and their vibrational normal modes were obtained from time-dependent DFT (TD-DFT) response theory. For the absorption and electronic circular dichroism spectra we calculated the 200 lowest-energy vertical spin-allowed electronic excitations. The transitions were subsequently Gaussian-broadened with σ = 0.20 eV to simulate the spectral envelopes. For overviews of the theoretical approach to model natural optical activity by quantum chemical calculations, in particular via TD-DFT, see, for example, available reviews.[75-76] Different functionals and the impact of solvent effects were tested for these compounds; see the ESI for details.

Photophysical and chiroptical properties of 2, 3 and 4. The two tetracarbazole systems show similar UV-vis absorption spectra as dimer **4**, with a broad and intense band at 310 nm (ε ~ 6-7 × 10^4 M^{-1} cm^{-1}), and a less intense band in the low energy region between 340 and 400 nm (ε ~ 1-2 × 10^4 M^{-1} cm^{-1}), displaying a vibronic progression (Figure 2). This optical signature is similar to their common precursor **1**, more so for **2** than **3**, as expected based on the carbazole isomerism found in these compounds. Indeed, **2** is a direct dimer of **1** while **3** can be viewed better as a dimer of **4**. Both for **2** and **3**, some electronic interaction between the two fragments is indicated by the 20 nm red-shift observed in the low-energy region of the absorption spectra in comparison to **1** and **4**. For both tetracarbazole compounds, the lowest-energy excitation with sizeable oscillator strength *f* corresponds to the HOMO-LUMO transition at 388 and 378 nm for **2** and **3** respectively. For **2**, the HOMO is mainly localized on the biaryl fragments of the 6,6'-bicarbazole system, extending over the nitrogen and oxygen atoms. The LUMO and LUMO+1 are localized on either 4,4'-bicarbazole unit and display a small energy difference of 0.120 eV. For **3**, the HOMO and HOMO-1 are almost degenerate (ΔE = 0.086 eV), and mostly localized on either of the two methoxy carbazole fragments at each extremity of the helix with a small contribution on the inner 4,4'-bicarbazole system, in which the LUMO is exclusively localized. Visual inspection of the corresponding MO isosurface plots reveals that the HOMO-1 and HOMO are essentially in-phase and out-of-phase (+/-) linear combinations of carbazole fragment frontier orbitals (FFOs), indicating a weak electronic interaction between the two 4,4'-bicarbazole units for **3**. The chiroptical properties of **2** and **3** have also been characterized, both experimentally and theoretically, as detailed in the Supporting Information (Figures S5-6 and S46).

Tetracarbazoles **2** and **3** display moderately intense fluorescence around 400-450 nm (Figure 2), with similar photoluminescence quantum yields of ~20%. The emission of **2** appears slightly structured, as in the case of **1**, with a maximum at 426 nm and blue-shifted in comparison to **3**. The latter displays a broader luminescence profile centered at 450 nm, close to the one obtained for model **4**, which further confirms the difference of electronic interaction between the carbazole units in **2** and **3**. Corresponding mirror-image CPL spectra were obtained for both pairs of enantiomers (Figure S5).

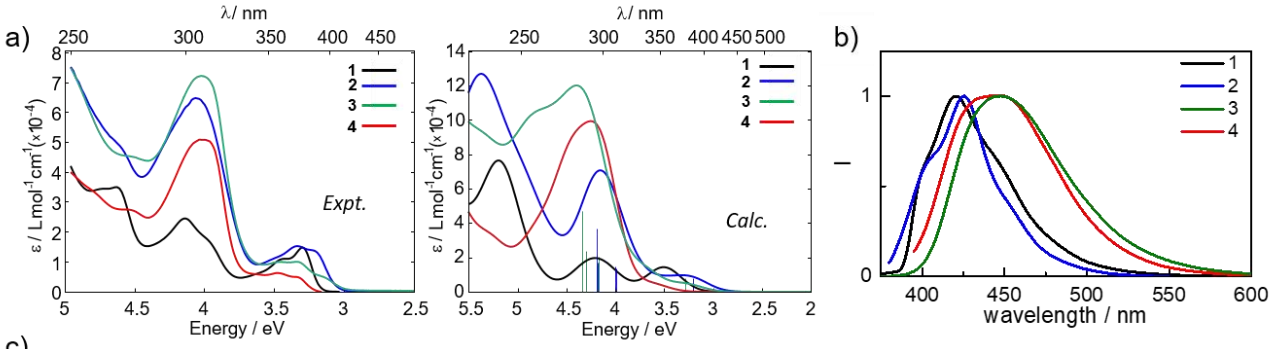

c)

Excit-ation	λ [nm]	f	occ. no.	unocc no.	%
			(+)-2		
#1	388	0.076	H	L	46
#9	310	0.124	H-5	L	28
#11	308	0.134	H	L+2	23
#14	298	0.143	H-4	L+1	14
#15	297	0.358	H	L+4	33
			(+)-3		
#1	378	0.066	H	L	45
#14	298	0.212	H-3 H-2	L+1 L+2	22 15
#16	289	0.250	H	L+4	32
#17	287	0.498	H-1 H	L+4 L+5	19 15

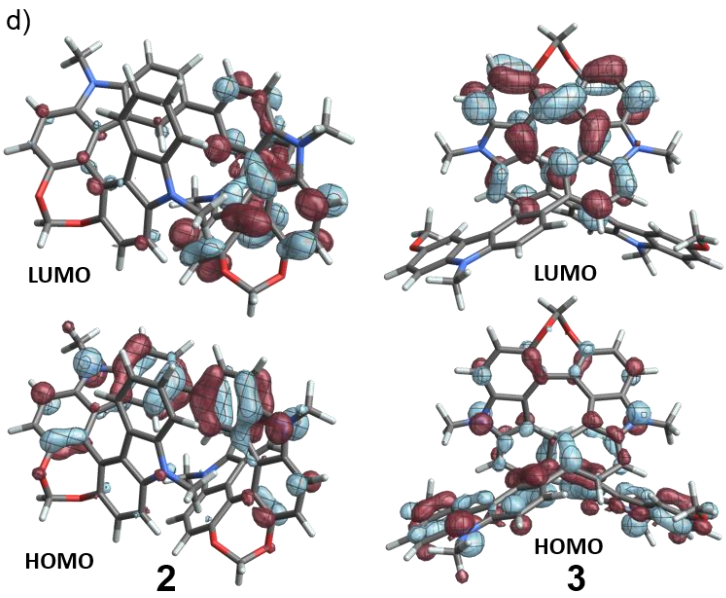

Figure 2. a) Experimental and calculated UV−vis absorption spectra of **1** (black), **2** (blue), **3** (green) and **4** (red) in dichloromethane at 298 K, selected transitions and oscillator strengths are indicated by 'sticks'; b) Normalized fluorescence spectra of **1** (black), **2** (blue), **3** (green) and **4** (red) in dichloromethane at 298 K; c) Details for selected transitions and occupied (occ)-unoccupied (unocc) MO pair contributions (greater than 10%) to the transition density for (+)-**2** and (+)-**3**. H and L indicate the HOMO and LUMO, respectively. d) Isosurfaces of HOMO and LUMO for **2** and **3** (±0.035 a.u.).

Radicals $2^{\bullet+}$, $3^{\bullet+}$ and $4^{\bullet+}$. Cyclic voltammetry (CV) of **2** and **3** revealed multiple reversible oxidation processes related to the presence of the four carbazole units. In comparison to bicarbazole **1**, which shows only two irreversible oxidation signals at +1.14 and +1.40 V, as classically observed for 3- and/or 6-unprotected carbazole derivatives,[64, 77-78] **2** displays three reversible oxidation events at 0.85, 1.17, and 1.3 V (*vs.* SCE, Figure 3), which, for the latter, corresponds to a two-oxidation process (Figure S8). Compound **3** exhibits two consecutive sets of two one-oxidation processes at 0.84 and 0.93 V, and at 1.23 and 1.27 V *vs.* SCE. In comparison to **1**, the presence of additional anodic potentials for **2** and **3** can be attributed to the 6,6'bicarbazole connection, as confirmed by the CV of model **4**, which shows one reversible oxidation at 0.71 V, followed by an irreversible one at *ca.* 1.11 V (*vs.* SCE, Figure 3). It is therefore interesting to note the difference of reversibility observed for the oxidation events when compared **2** and **3**, to **1** and **4**, highlighting the important role of the peripheral carbazole substituents around the 6,6'-bicarbazole fragment.

This aspect is further confirmed by investigating the corresponding monoradicals $\mathbf{2}^{\bullet+}$ $\mathbf{SbCl_6}^-$, $\mathbf{3}^{\bullet+}$ $\mathbf{SbCl_6}^-$ and $\mathbf{4}^{\bullet+}$ $\mathbf{SbCl_6}^-$, using tris(4-bromophenyl)ammoniumyl hexachloridoantimonate ("magic blue" oxidant, Mb, 4-BrPh)$_3$NSbCl$_6$).[79] While **1** afforded instantaneously a mixture of dimeric and oligomeric species,[62] the other radicals can be quantitatively obtained in dichloromethane solutions at room temperature. The three persistent open-shell compounds display similar UV-vis-NIR absorption spectra including notably a broad NIR signature from 800 nm to up to 2000 nm (ε ~ 7-12 × 10^3 M^{-1} cm^{-1}, Figure 3). The latter is composed of three main bands found at 900, 1500 and 1700-2000 nm, and is attributed to transitions mainly involving the 6,6'-bicarbazole fragment. Electron paramagnetic resonance (EPR) measurements show an intense doublet signal of an organic based radical for each compound (g = 2.00, Figure 3 and Figure S25), also indicating a close similarity between the monoradicals. In air-saturated CH_2Cl_2, the half-life of $\mathbf{2}^{\bullet+}$ $\mathbf{SbCl_6}^-$, $\mathbf{3}^{\bullet+}$ $\mathbf{SbCl_6}^-$ and $\mathbf{4}^{\bullet+}$ $\mathbf{SbCl_6}^-$ has been determined to be 3.1 days, 17.5 and 6.5 hours, respectively. These large differences clearly highlight the impact of carbazole isomerism on the stability of these novel organic open-shell compounds. It is important to note that helical $\mathbf{3}^{\bullet+}$ $\mathbf{SbCl_6}^-$ and $\mathbf{4}^{\bullet+}$ $\mathbf{SbCl_6}^-$ show significant stability despite the lack of hindered *tert*-butyl groups, in comparison to sterically protected but unstable bicarbazole $\mathbf{1a}^{\bullet+}$ $\mathbf{SbCl_6}^-$ (Figure 1b). As suggested by the successful generation of $\mathbf{4}^{\bullet+}$ $\mathbf{SbCl_6}^-$, the 6,6'-bicarbazole connection seems to play a crucial role regarding the monoradical stability, presumably owing to the extended electronic delocalization of the un-

paired electron over the two carbazole units. In dichloromethane solution, a three-fold increase of half-life is reached for **3**$^{\bullet+}$ **SbCl$_6^-$** in comparison to **4**$^{\bullet+}$ **SbCl$_6^-$**, indicating an important steric and/or electronic impact of the second helical arm on the radical persistence. This aspect is even more pronounced for **2**$^{\bullet+}$ **SbCl$_6^-$** owing to the two peripheral carbazole fragments surrounding the 6,6'bicarbazole fragments.

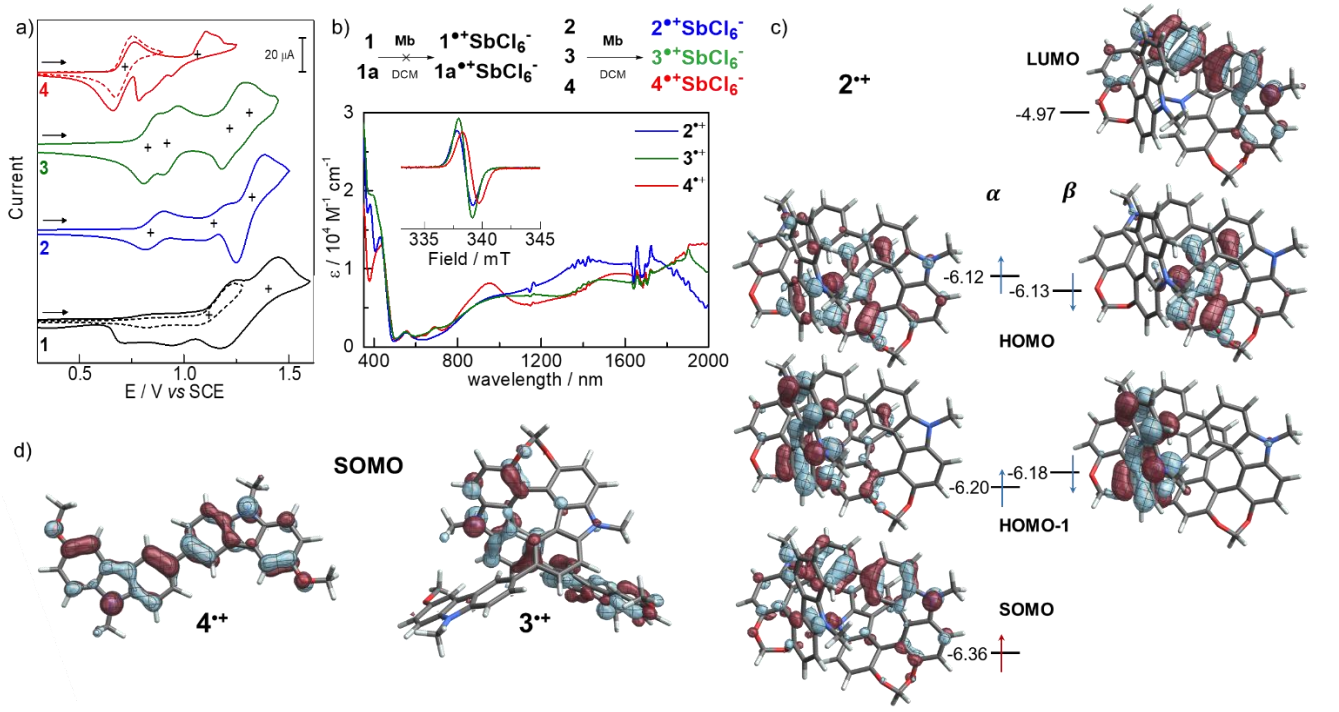

Figure 3. a) Cyclic voltammograms (CVs) of **1** (black), **2** (blue), **3** (green), and **4** (red) *versus* saturated calomel electrode (SCE) as the reference and 0.2 M Bu_4NPF_6 in dichloromethane with ferrocene as internal standard; b) Synthetic route to persistent radical **2**$^{\bullet+}$ **SbCl$_6^-$** (blue), **3**$^{\bullet+}$ **SbCl$_6^-$** (green), and **4**$^{\bullet+}$ **SbCl$_6^-$** (red) with corresponding UV-vis-NIR absorption spectra of **2**$^{\bullet+}$**SbCl$_6^-$** (blue), **3**$^{\bullet+}$ **SbCl$_6^-$** (green), and **4**$^{\bullet+}$ **SbCl$_6^-$** (red) in dichloromethane at 298 K; inset: X-band EPR (ν = 9.4858 GHz) of **2**$^{\bullet+}$ **SbCl$_6^-$** (blue), **3**$^{\bullet+}$ **SbCl$_6^-$** (green), and **4**$^{\bullet+}$ **SbCl$_6^-$** (red) in dichloromethane at 298 K; c) Isosurfaces (±0.030 a.u.) of frontier molecular orbitals computed for monoradicals **2**$^{\bullet+}$, and d) Isosurfaces (±0.030 a.u.) of SOMO for monoradicals **3**$^{\bullet+}$, and **4**$^{\bullet+}$.

Theoretical calculations using spin-unrestricted Kohn-Sham (KS) DFT help to rationalize the observations. Visual inspection of the MO isosurface plots of **2**$^{\bullet+}$, **3**$^{\bullet+}$ and **4**$^{\bullet+}$ confirms that, for each compound, the SOMO and the corresponding β-spin hole represented by the LUMO are indeed localized on the 6,6'-bicarbazole fragment, with almost no contributions of the other carbazole unit for **2**$^{\bullet+}$ and **3**$^{\bullet+}$ (Figure 3). However, these additional donor fragments seem to play a crucial role for the radical stability, as indicated by the half-life values. Indeed, both **2**$^{\bullet+}$ and **3**$^{\bullet+}$ show a peculiar electronic configuration since their SOMOs are lower in energy than the HOMO and HOMO-1, localized on the non-oxidized carbazole fragments for each monoradicals (Figure 3 for **2**$^{\bullet+}$ and S54 for **3**$^{\bullet+}$). The calculated orbital energy gap ΔE between the HOMO and the SOMO is 0.24 eV and 0.59 eV for **2**$^{\bullet+}$ and **3**$^{\bullet+}$, respectively, indicating a stronger interaction between the radical center and the external carbazole units in **2**$^{\bullet+}$. This is also confirmed by the larger energy difference between the HOMO of **2** and **2**$^{\bullet+}$, *ca.* 0.80 eV, as compared to 0.31 eV for **3** and **3**$^{\bullet+}$. This can be explained for the latter by the larger spatial separation of the SOMO and the HOMO, localized on the opposite 3-methoxycarbazole fragment (Figure S54). Importantly, **4**$^{\bullet+}$ shows nearly degenerate SOMO - β-spin HOMO energy levels, while the α-spin HOMO is almost 0.4 eV lower in energy (Figure S56), further highlighting the importance of the dihedral angle at the 4,4-bicarbazole connection in helical **2**$^{\bullet+}$ **SbCl$_6^-$** and **3**$^{\bullet+}$ **SbCl$_6^-$** to promote SHI efficiently.

As mentioned before, SHI has been claimed as a stabilizing strategy for radicals,[27-30, 37, 80] and our results suggest that this effect is also responsible for the observed increase of stability when going from **4**$^{\bullet+}$**SbCl$_6^-$** to **3**$^{\bullet+}$ **SbCl$_6^-$**, and further to **2**$^{\bullet+}$ **SbCl$_6^-$**, in which the additional carbazole fragments stabilize both electronically and sterically the unpaired electron localized on the 6,6'-bicarbazole unit.

Beyond being new examples of chiral monoradicals with SHI, the unique donor-acceptor type structure of both **2**$^{\bullet+}$**SbCl$_6^-$** and **3**$^{\bullet+}$ **SbCl$_6^-$**, combined with their persistence, presents an exciting opportunity to study the potential intramolecular electron transfer (IET) that may occur between the spin center and the additional carbazole donor units.[81] Investigating this aspect in the context of chiral open-shell compounds is of high interest given the unique ability of chiral molecules to filter the spin of electron upon charge conduction (*e.g.* chirality-induced-spin-selectivity, CISS).[82-85] We gained insight into IET by recording the optical signatures of **2**$^{\bullet+}$ **SbCl$_6^-$** and **3**$^{\bullet+}$ **SbCl$_6^-$** in polar solvent such as acetonitrile. As depicted in Figure 4, the UV-vis-NIR absorption spectrum of **2**$^{\bullet+}$**SbCl$_6^-$** displays significant differences compared to the one obtained in dichloromethane, notably a strong decrease of the NIR intensity between 1000 and 2000 nm, and decreased band intensity at 410 and 550 nm, along with an 80 nm blue shift of the band at 970 nm, which now dominates the optical response in the low energy region. The absorption spectrum of **3**$^{\bullet+}$**SbCl$_6^-$** in acetonitrile shows much less variation with only a slight decrease of the absorption

band around 1900 nm. These changes in function of the solvent polarity indicate that spin delocalization occurs in both systems, as generally observed for class II of organic mixed valence (MV) compounds (Figure S10 and ESI for more details).[86-88]

Both **2**$^{\bullet+}$ **SbCl$_6^-$** and **3**$^{\bullet+}$ **SbCl$_6^-$** remain also configurationally stable, which allowed us to gather additional information on the spin delocalization within the chiral π-conjugated system by recording the ECD of both **2**$^{\bullet+}$ **SbCl$_6^-$** and **3**$^{\bullet+}$ **SbCl$_6^-$** in solvents of different polarity (Figure 4). In dichloromethane, enantiomers of both **2**$^{\bullet+}$ **SbCl$_6^-$** and **3**$^{\bullet+}$ **SbCl$_6^-$** show expected mirror-image spectra associated with radical absorption transitions across the visible and the NIR region (Figure 4). Radical (+)-**2**$^{\bullet+}$ **SbCl$_6^-$** displays a positive signal at 550 nm ($\Delta\varepsilon$ = + 3.0 M^{-1} cm^{-1}), followed by a broad negative one between 600 and 1000 nm ($\Delta\varepsilon$ = - 2.0 M^{-1} cm^{-1}). For (+)-**3**$^{\bullet+}$ **SbCl$_6^-$**, a positive signal is observed at 460 nm ($\Delta\varepsilon$ = - 1.1 M^{-1} cm^{-1}), two negative and positive ones at 510 and 580 nm ($|\Delta\varepsilon|$ = 0.5 M^{-1} cm^{-1}), respectively, and finally a very broad positive band until 1000 nm ($\Delta\varepsilon$ = + 2.3 M^{-1} cm^{-1}). Changing the solvent to acetonitrile impacts the ECD of both monoradicals with a 70 nm blue-shift of the band observed at 620 nm in dichloromethane for (+)-**2**$^{\bullet+}$ **SbCl$_6^-$**. The ECD of (+)-**3**$^{\bullet+}$ **SbCl$_6^-$** appears more impacted by the solvent environment since a new band appears at 940 nm with the ECD between 650 and 920 nm being opposite in sign to the ECD recorded in dichloromethane (Figure 4). To the best of our knowledge, this is the first evidence of ECD sign inversion for chiral organic radicals as a function of solvent polarity. A simple continuum solvent model in the calculations did not produce the sign change, which means that the dielectric constant of the solvent alone is not sufficient to rationalize this intriguing effect. We tentatively assign the sign change to a combination of solvent polarity and dynamics. Finally, the lifetimes of **2**$^{\bullet+}$ **SbCl$_6^-$** and **3**$^{\bullet+}$ **SbCl$_6^-$** have been also monitored in acetonitrile, showing half-life values of less than one hour for both compounds, a dramatic decrease in comparison to the ones obtained in dichloromethane (Figure 4c).

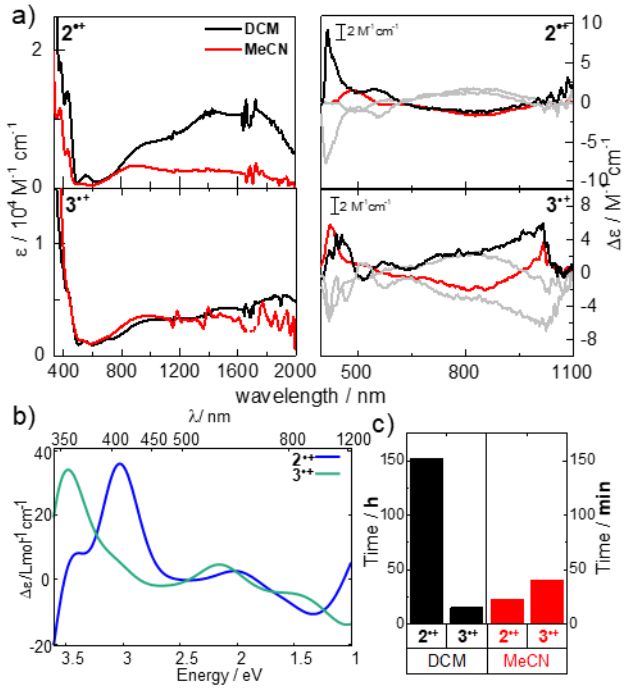

Figure 4. a) Left: UV spectra of **2**$^{\bullet+}$ **SbCl$_6^-$** (top) and **3**$^{\bullet+}$ **SbCl$_6^-$** (bottom) in dichloromethane (black) and acetonitrile (blue) at 298 K. right: vis-NIR ECD spectra of (+)-**2**$^{\bullet+}$ **SbCl$_6^-$** (top) and (+)-**3**$^{\bullet+}$ **SbCl$_6^-$** (bottom) in dichloromethane (black) and acetonitrile (blue) at 298 K with their corresponding (-) and (-) enantiomers in grey. b) Calculated ECD spectra of (+)-**2**$^{\bullet+}$ **SbCl$_6^-$** (blue) and (+)-**3**$^{\bullet+}$ **SbCl$_6^-$** (green) with PCM for dichloromethane solvent; c) Half-life time values ($t_{1/2}$) of **2**$^{\bullet+}$ **SbCl$_6^-$** and **3**$^{\bullet+}$ **SbCl$_6^-$** in dichloromethane (DCM) and acetonitrile (MeCN) under air atmosphere at 298 K.

Diradicals 2$^{2\bullet2+}$ 2SbCl$_6^-$ and 3$^{2\bullet2+}$ 2SbCl$_6^-$, and related characterizations. Having these innovative helical SHI monoradicals available allowed us to generate the corresponding diradicals and investigate the chiroptical and magnetic properties resulting from the presence of two unpaired electrons within these chiral systems. Following previous examples in the literature,[17, 32-33, 89] oxidation of an SHI monoradical may result in a diradical with triplet ground state multiplicity or an open-shell singlet with antiferromagnetic coupling of the unpaired spins. Calculations predict the singlet and triplet spin configurations of the doubly oxidized compounds **2**$^{2\bullet2+}$ **2SbCl$_6^-$**, **3**$^{2\bullet2+}$ **2SbCl$_6^-$** and **4**$^{2\bullet2+}$ **2SbCl$_6^-$** to be close in energy, as expected, with the antiferromagnetically coupled singlets being slightly lower in energy (Tables S16-S18) or effectively isoenergetic with the triplet (for **3**$^{2\bullet2+}$). The estimated singlet-triplet energy gaps (ΔE_{ST}) are -0.57, -0.04 and -0.84 kcal mol^{-1} for diradicals **2**$^{2\bullet2+}$, **3**$^{2\bullet2+}$ and **4**$^{2\bullet2+}$, respectively, with the PBE0 functional (Table S19). Whereas the formation of **4**$^{2\bullet2+}$ **2SbCl$_6^-$** results instantaneously in the formation of polymeric mixture (Figure S11), as anticipated by the non-fully reversible second oxidation process of **4** observed in CV (Figure 3), **2**$^{2\bullet2+}$ **2SbCl$_6^-$** and **3**$^{2\bullet2+}$ **2SbCl$_6^-$** can be quantitatively obtained upon addition of one equivalent of magic blue to dichloromethane solutions of **2**$^{\bullet+}$ **2SbCl$_6^-$** or **3**$^{\bullet+}$ **2SbCl$_6^-$** monoradicals, or directly from neutral **2** and **3** using two equivalents of oxidant. The difference of stability between the three diradicals clearly highlights the crucial role of the two additional carbazole units for generating persistent **2**$^{2\bullet2+}$ **2SbCl$_6^-$** and **3**$^{2\bullet2+}$ **2SbCl$_6^-$**, which represent two innovative examples of helical diradicals.[31] In dichloromethane solution (Figure 5), **2**$^{2\bullet2+}$ **2SbCl$_6^-$** displays a similar UV-vis-NIR signature than **2**$^{\bullet+}$ **SbCl$_6^-$**, with expected higher absorption intensity from the presence of additional oxidized carbazole units. The optical signature of **3**$^{2\bullet2+}$ **SbCl$_6^-$** shows a more structured profile in the NIR region than the one obtained for its monoradical counterpart, along with a marked absorption increase at 450 nm (ε = 15 000 M^{-1}cm^{-1} at 450 nm). The calculated spectra of **2**$^{2\bullet2+}$ and **3**$^{2\bullet2+}$ reproduced well the experimental ones and allowed us to assign the low-energy bands between 700 and 1200 nm to transitions among the set HOMO-1, HOMO and LUMO, LUMO+1 (Figure 5, S58-61, S63 and Table S20-23). More than being chemically persistent, enantiomers of **2**$^{2\bullet2+}$ **2SbCl$_6^-$** and **3**$^{2\bullet2+}$ **2SbCl$_6^-$** remain also configurationally stable. The corresponding mirror-image ECD spectra show similar profile than the ones obtained for **2**$^{\bullet+}$ **SbCl$_6^-$** and **3**$^{\bullet+}$ **SbCl$_6^-$**, with absorption anisotropy factors, $|g_{abs}|$, reaching 1.0 × 10^{-3} in the NIR region, among the highest measured for molecular organic diradicals.[31, 46]

EPR measurements on both **2**$^{2\bullet2+}$ **2SbCl$_6^-$** and **3**$^{2\bullet2+}$ **2SbCl$_6^-$** afforded a doublet signal at 77 and 298 K, neither displaying hyperfine coupling nor a Δm = 2 half-field transition, presumably due to a weak interaction between the two unpaired electrons (g = 2.00, Figure S27).[90] For each diradical, the EPR signal intensity decreases when lowering the temperature (Figure 5 and S30). Following the evolution of the product of integrated EPR

signal intensity and temperature (*i.e.* I × T) in function of the temperature in frozen dichloromethane solution allows us to characterize an antiferromagnetic coupling between the spins, with an estimated singlet-triplet gap (ΔE_{ST}) of -1.15 and -1.26 kcal mol^{-1} for $\mathbf{2^{2\bullet2+}}$ $\mathbf{2SbCl_6^-}$ and $\mathbf{3^{2\bullet2+}}$ $\mathbf{2SbCl_6^-}$, respectively, using the Bleaney-Bowers equation (Figure 5, the ΔE_{ST} gap values are the average of two different measurments, see ESI for details).[91] These results confirm the expected formation of a diradical upon oxidation of the highest doubly occupied molecular orbital for both $\mathbf{2^{2\bullet2+}}$ $\mathbf{2SbCl_6^-}$ and $\mathbf{3^{2\bullet2+}}$ $\mathbf{2SbCl_6^-}$, as expected from the SHI electronic configuration of the monoradicals.[62] Calculations show that for $\mathbf{2^{2\bullet2+}}$ $\mathbf{2SbCl_6^-}$, both in the triplet and open-shell singlet configuration, one SOMO is localized on the biaryl fragment of the 6,6'-bicarbazole π-conjugated system, while the other one is localized on the helical 4,4'-bicarbazole fragments, indicating therefore a weak interaction between the unpaired electrons.[30, 40] A similar situation is also obtained for $\mathbf{3^{2\bullet2+}}$•$\mathbf{2SbCl_6^-}$, because the two SOMOs are spread out over each 6,6'-bicarbazole fragments (Figure S61). Visual inspection of the two SOMOs confirms a weak spatial overlap of these two orbitals, which can be thus considered as disjoint (Figure 5). As a result of the spatial separation, the exchange repulsion integral between the two unpaired MOs is going to be small and not necessarily the decisive factor in the stabilization of a triplet vs. singlet electronic configuration, such that ultimately a singlet ground state is favored, contrary to Hund's rule expectations.[4, 92] The present calculations agree with the experiments in that the singlet diradical configurations are favoured over the triplets, as long as the singlets are calculated in the usual 'broken symmetry' (BS) fashion.[93] $\langle \hat{S}^2 \rangle$ values from the BS calculations, given in Tables S16—S18, are approximately 1, which is expected,[93] and reflects the presence of two weakly interacting radical centers. The triplet $\langle \hat{S}^2 \rangle$ values are close to the idealized 2 and do not raise concerns regarding spin contamination. As a check, similar calculations were performed for the bi-radical of a previous related study,[62] and we also obtained close energies between the BS singlet and the triplet, with the singlet being very slightly lower in energy in agreement with experiments. Irrespective of the spin multiplicity of the present diradicals, the two SOMOs are unexpectedly separated energetically from the highest occupied level by other sets of spin-paired orbitals (Figure 5 and S60-61). While a recent theoretical study of Abe *et al.* has proposed a diradical system showing SHI between HOMO and SOMO-1 levels,[94] the electronic configuration of SHI diradical $\mathbf{2^{2\bullet2+}}$ appears particularly intriguing. Experiments and calculations suggest that the occurrence of a spatially disjoint pair of MOs energetically below the highest occupied level may contribute to the diradical stability.

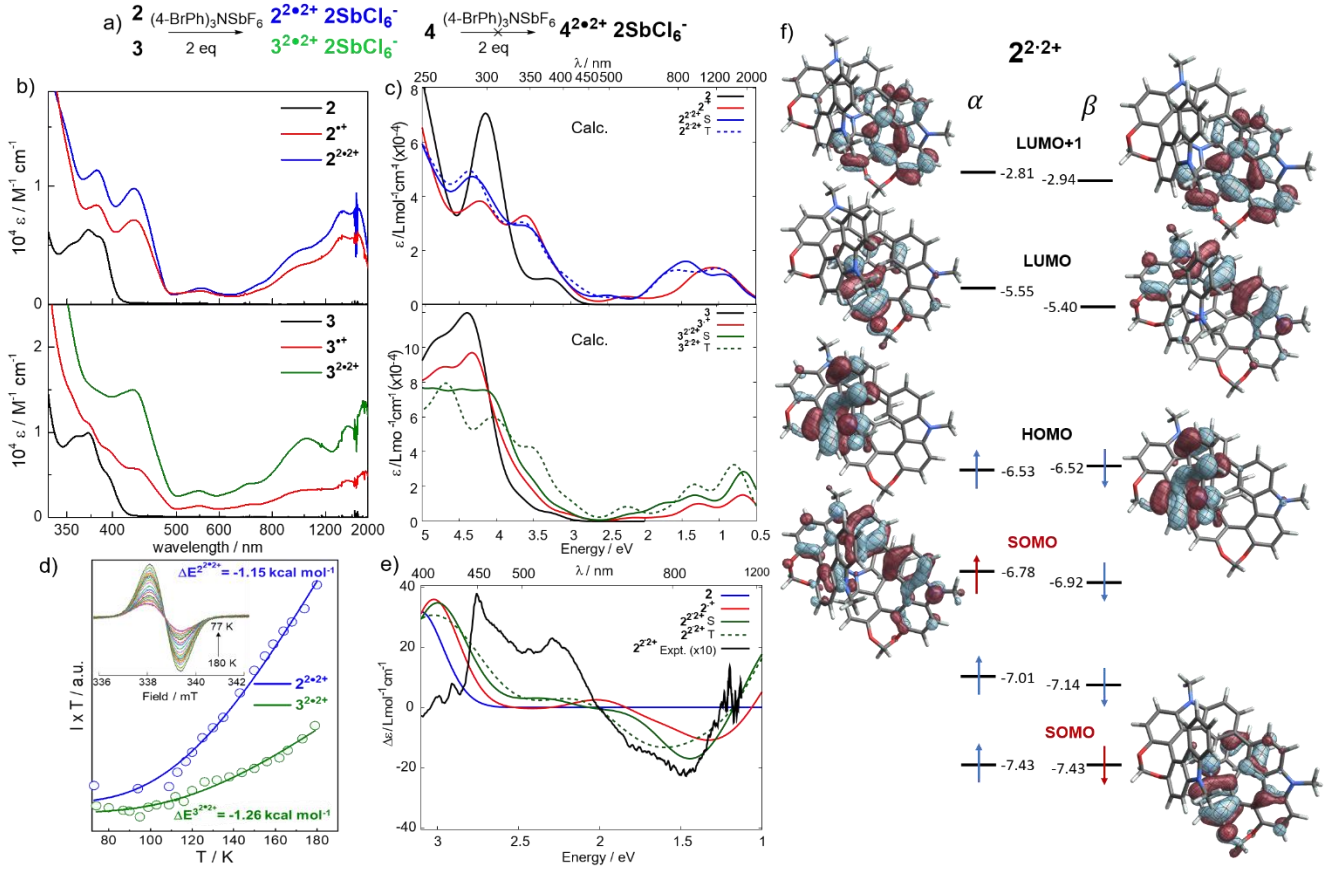

Figure 5. a) Synthetic route to persistent radicals $\mathbf{2^{2\bullet2+}}$ $\mathbf{2SbCl_6^-}$, $\mathbf{3^{2\bullet2+}}$ $\mathbf{2SbCl_6^-}$, and $\mathbf{4^{2\bullet2+}}$ $\mathbf{2SbCl_6^-}$. b) UV-vis-NIR absorption spectra of: **2** (black), $\mathbf{2^{\bullet+}}$ $\mathbf{SbCl_6^-}$ (red) and $\mathbf{2^{2\bullet2+}}$ $\mathbf{2SbCl_6^-}$ (blue) (top), and **3** (black), $\mathbf{3^{\bullet+}}$ $\mathbf{SbCl_6^-}$ (red) and $\mathbf{3^{2\bullet2+}}$ $\mathbf{2SbCl_6^-}$ (green) (bottom) in dichloromethane at 298 K; c) Calculated UV-vis-NIR absorption spectra of top: **2** (black), $\mathbf{2^{\bullet+}}$ $\mathbf{SbCl_6^-}$ (red) (top), and $\mathbf{2^{2\bullet2+}}$ $\mathbf{2SbCl_6^-}$ (blue) and bottom: **3** (black), $\mathbf{3^{\bullet+}}$ $\mathbf{SbCl_6^-}$ (red) and $\mathbf{3^{2\bullet2+}}$ $\mathbf{2SbCl_6^-}$ (green) in dichloromethane. d) IT *vs*. T plots of frozen solution of diradicals $\mathbf{2^{2\bullet2+}}$ $\mathbf{2SbCl_6^-}$ (blue) and $\mathbf{3^{2\bullet2+}}$ $\mathbf{2SbCl_6^-}$ (green) in dichloromethane fitted using Bleaney-Bowers model with an estimated average $\Delta E_{S\text{-}T}$ values obtained from two measurements. e) Experimental vis-NIR ECD spectrum of $\mathbf{2^{2\bullet2+}}$•$\mathbf{2SbCl_6^-}$ (black) and calculated vis-NIR ECD spectra of (+)-**2** (blue), (+)-$\mathbf{2^{\bullet+}}$ (red) and (+)-$\mathbf{2^{2\bullet2+}}$ (green) for both singlet (solid line) and triplet (dashed line) spin multiplicity; f) Top: Isosurfaces (±0.030 a.u.) of frontier molecular orbitals computed for diradicals $\mathbf{2^{2\bullet2+}}$.

CONCLUSION

In conclusion, we have reported the synthesis, characterization, and computational analysis of a new series of carbazole-based persistent chiral open-shell systems. The obtained mono- and diradicals are persistent, show configurational stability and SHI in both cases, allowing us to characterize in depth their chiroptical and magnetic properties. In comparison to the previously reported unstable helical bicarbazole radical, we show that extending the delocalization of the unpaired electrons within the helical π-conjugated system strongly increases the chemical stability of the monoradicals and creates intense CP-light absorption in the near infra-red region. Interestingly, modifying the molecular arrangement of the carbazole units impacts both the optical and chiroptical properties of the open-shell systems, as well as their persistent character, with half-life up to several days in solution at room temperature. Along with these new findings, we also investigated the IET that occurs within the chiral monoradicals and show for the first time that increasing the polarity of the medium can lead to ECD sign inversion of the radical absorption transitions. Investigating this IET aspect in the context of chiral open-shell compounds is of high interest given the unique ability of chiral molecules to filter the spin of electron upon charge conduction (*e.g.* chirality-induced-spin-selectivity, CISS).[82-85] Finally, we successfully generated two innovative chiral diradicals, which bring new aspects regarding the structural and electronic parameters impacting the stability, optical and chiroptical of such scarce chiral open-shell systems. The obtained persistent compounds show an antiferromagnetic interaction between the unpaired electrons in the experiments, and an intriguing electronic configuration with also a SHI in the diradical state. While the consequences of this unprecedented result remain to be explored, its potential impact on the unpaired electrons exchange/repulsion, orbital relaxation contributions are of fundamental interest for exploring organic polyradical systems. It is our hope that these results may help in designing new (chiral) open-shell systems with higher persistent character and a better control of the organic spins interaction.

ASSOCIATED CONTENT

Supporting Information. Methods and synthetic procedures, ORTEP diagrams, table of crystal data, unit cell diagrams, chiral stationary phase HPLC separation data, additional photophysical and chiroptical characterizations and theoretical calculations can be found in the Electronic Supporting Information.

CORRESPONDING AUTHORS

* jochena@buffalo.edu
* ludovic.favereau@univ-rennes1.fr

NOTES

The authors declare no competing financial interest.

ACKNOWLEDGMENT

We acknowledge the Ministère de l'Enseignement supérieur, de la Recherche et de l'Innovation, the Centre National de la Recherche Scientifique (CNRS). L.F. thanks the French National Research Agency (ANR) for financial support (OChiRaLec project, ANR-ANR-21-CE07-0019-01). J. A. thanks the National Science Foundation (CHE-1855470) for financial support of the computational component of this study, and the Center for Computational Research (CCR) at the University at Buffalo for providing computational resources.[95] Part of this work has been performed using the Spectroscopies-CDTP core facility (UMS Biosit, Univ Rennes, RENNES, FRANCE).

REFERENCES

1. Ardenkjær-Larsen, J. H.; Fridlund, B.; Gram, A.; Hansson, G.; Hansson, L.; Lerche, M. H.; Servin, R.; Thaning, M.; Golman, K., Increase in signal-to-noise ratio of > 10,000 times in liquid-state NMR. *Proc. Natl. Acad. Sci. U. S. A.* **2003**, *100* (18), 10158-10163.
2. B. B. Williams; H. J. Halpern, *Biomedical EPR - Part A: Free Radicals, Metals, Medicine and Physiology*. Springer US: 2005.
3. Mathies, G.; Caporini, M. A.; Michaelis, V. K.; Liu, Y.; Hu, K.-N.; Mance, D.; Zweier, J. L.; Rosay, M.; Baldus, M.; Griffin, R. G., Efficient Dynamic Nuclear Polarization at 800 MHz/527 GHz with Trityl-Nitroxide Biradicals. *Angew. Chem. Int. Ed.* **2015**, *54* (40), 11770-11774.
4. Abe, M., Diradicals. *Chem. Rev.* **2013**, *113* (9), 7011-7088.
5. Zeng, Z.; Shi, X.; Chi, C.; López Navarrete, J. T.; Casado, J.; Wu, J., Pro-aromatic and anti-aromatic π-conjugated molecules: an irresistible wish to be diradicals. *Chem. Soc. Rev.* **2015**, *44* (18), 6578-6596.
6. Kumar, S.; Kumar, Y.; Keshri, S. K.; Mukhopadhyay, P., Recent Advances in Organic Radicals and Their Magnetism. *Magnetochemistry* **2016**, *2* (4), 42.
7. Hu, X.; Wang, W.; Wang, D.; Zheng, Y., The electronic applications of stable diradicaloids: present and future. *J. Mater. Chem. C* **2018**, *6* (42), 11232-11242.
8. Y. Gopalakrishna, T.; Zeng, W.; Lu, X.; Wu, J., From open-shell singlet diradicaloids to polyradicaloids. *Chem. Commun.* **2018,** *54* (18), 2186-2199.
9. Kato, K.; Osuka, A., Platforms for Stable Carbon-Centered Radicals. *Angew. Chem. Int. Ed.* **2019**, *58* (27), 8978-8986.
10. Ni, Y.; Gopalakrishna, T. Y.; Phan, H.; Kim, T.; Herng, T. S.; Han, Y.; Tao, T.; Ding, J.; Kim, D.; Wu, J., 3D global aromaticity in a fully conjugated diradicaloid cage at different oxidation states. *Nat. Chem.* **2020**, *12* (3), 242-248.
11. Liu, C.; Ni, Y.; Lu, X.; Li, G.; Wu, J., Global Aromaticity in Macrocyclic Polyradicaloids: Huckel's Rule or Baird's Rule? *Acc Chem Res* **2019**, *52* (8), 2309-2321.
12. Peng, Q.; Obolda, A.; Zhang, M.; Li, F., Organic Light-Emitting Diodes Using a Neutral π Radical as Emitter: The Emission from a Doublet. *Angew. Chem. Int. Ed.* **2015**, *54* (24), 7091-7095.
13. Gu, X.; Gopalakrishna, T. Y.; Phan, H.; Ni, Y.; Herng, T. S.; Ding, J.; Wu, J., A Three-Dimensionally π-Conjugated Diradical Molecular Cage. *Angew. Chem. Int. Ed.* **2017**, *56* (48), 15383-15387.
14. Ai, X.; Chen, Y.; Feng, Y.; Li, F., A Stable Room-Temperature Luminescent Biphenylmethyl Radical. *Angew. Chem. Int. Ed.* **2018**, *57* (11), 2869-2873.
15. Ai, X.; Evans, E. W.; Dong, S.; Gillett, A. J.; Guo, H.; Chen, Y.; Hele, T. J. H.; Friend, R. H.; Li, F., Efficient radical-based light-emitting diodes with doublet emission. *Nature* **2018**, *563* (7732), 536-540.
16. Sugawara, T.; Matsushita, M. M., Spintronics in organic π-electronic systems. *J. Mater. Chem.* **2009**, *19* (12), 1738-1753.
17. Sugawara, T.; Komatsu, H.; Suzuki, K., Interplay between magnetism and conductivity derived from spin-polarized donor radicals. *Chem. Soc. Rev.* **2011**, *40* (6), 3105-3118.

18. Yuan, D.; Liu, W.; Zhu, X., Design and Applications of Single-Component Radical Conductors. *Chem* **2021**, *7* (2), 333-357.
19. Tan, Y.; Casetti, N. C.; Boudouris, B. W.; Savoie, B. M., Molecular Design Features for Charge Transport in Nonconjugated Radical Polymers. *J. Am. Chem. Soc.* **2021**, *143* (31), 11994-12002.
20. Kimura, S.; Matsuoka, R.; Kimura, S.; Nishihara, H.; Kusamoto, T., Radical-Based Coordination Polymers as a Platform for Magnetoluminescence. *J. Am. Chem. Soc.* **2021**, *143* (15), 5610-5615.
21. Medina Rivero, S.; Shang, R.; Hamada, H.; Yan, Q.; Tsuji, H.; Nakamura, E.; Casado, J., Non-Aufbau Spiro-Conjugated Quinoidal & Aromatic Charged Radicals. *Bull. Chem. Soc. Jpn.* **2021**, *94* (3), 989-996.
22. Ratera, I.; Vidal-Gancedo, J.; Maspoch, D.; Bromley, S. T.; Crivillers, N.; Mas-Torrent, M., Perspectives for polychlorinated trityl radicals. *J. Mater. Chem. C* **2021**, *9* (33), 10610-10623.
23. Shu, C.; Pink, M.; Junghoefer, T.; Nadler, E.; Rajca, S.; Casu, M. B.; Rajca, A., Synthesis and Thin Films of Thermally Robust Quartet (S = 3/2) Ground State Triradical. *J. Am. Chem. Soc.* **2021**, *143* (14), 5508-5518.
24. Calzolari, A.; Rajca, A.; Casu, M. B., From radical to triradical thin film processes: the Blatter radical derivatives. *J. Mater. Chem. C* **2021**, *9* (33), 10787-10793.
25. Chen, Z. X.; Li, Y.; Huang, F., Persistent and Stable Organic Radicals: Design, Synthesis, and Applications. *Chem* **2021**, *7* (2), 288-332.
26. Hudson, J. M.; Hele, T. J. H.; Evans, E. W., Efficient light-emitting diodes from organic radicals with doublet emission. *J. Appl. Phys.* **2021**, *129* (18), 180901.
27. Gryn'ova, G.; Marshall, D. L.; Blanksby, S. J.; Coote, M. L., Switching radical stability by pH-induced orbital conversion. *Nat. Chem.* **2013**, *5*, 474.
28. Franchi, P.; Mezzina, E.; Lucarini, M., SOMO–HOMO Conversion in Distonic Radical Anions: An Experimental Test in Solution by EPR Radical Equilibration Technique. *J. Am. Chem. Soc.* **2014**, *136* (4), 1250-1252.
29. Wang, Y.; Zhang, H.; Pink, M.; Olankitwanit, A.; Rajca, S.; Rajca, A., Radical Cation and Neutral Radical of Aza-thia[7]helicene with SOMO–HOMO Energy Level Inversion. *J. Am. Chem. Soc.* **2016**, *138* (23), 7298-7304.
30. Kumar, A.; Sevilla, M. D., SOMO–HOMO Level Inversion in Biologically Important Radicals. *J. Phys. Chem. B* **2018**, *122* (1), 98-105.
31. Shu, C.; Zhang, H.; Olankitwanit, A.; Rajca, S.; Rajca, A., High-Spin Diradical Dication of Chiral pi-Conjugated Double Helical Molecule. *J. Am. Chem. Soc.* **2019**, *141* (43), 17287-17294.
32. Izuoka, A.; Hiraishi, M.; Abe, T.; Sugawara, T.; Sato, K.; Takui, T., Spin Alignment in Singly Oxidized Spin-Polarized Diradical Donor: Thianthrene Bis(nitronyl nitroxide). *J. Am. Chem. Soc.* **2000**, *122* (13), 3234-3235.
33. Sakurai, H.; Izuoka, A.; Sugawara, T., Design, Preparation, and Electronic Structure of High-Spin Cation Diradicals Derived from Amine-Based Spin-Polarized Donors. *J. Am. Chem. Soc.* **2000**, *122* (40), 9723-9734.
34. Nakazaki, J.; Chung, I.; Matsushita, M. M.; Sugawara, T.; Watanabe, R.; Izuoka, A.; Kawada, Y., Design and preparation of pyrrole-based spin-polarized donors. *J. Mater. Chem.* **2003**, *13* (5), 1011-1022.
35. Komatsu, H.; Mogi, R.; Matsushita, M. M.; Miyagi, T.; Kawada, Y.; Sugawara, T., Synthesis and properties of TSF-based spin-polarized donor. *Polyhedron* **2009**, *28* (9), 1996-2000.
36. Souto, M.; Rovira, C.; Ratera, I.; Veciana, J., TTF–PTM dyads: from switched molecular self assembly in solution to radical conductors in solid state. *CrystEngComm* **2017**, *19* (2), 197-206.
37. Guo, H.; Peng, Q.; Chen, X.-K.; Gu, Q.; Dong, S.; Evans, E. W.; Gillett, A. J.; Ai, X.; Zhang, M.; Credgington, D.; Coropceanu, V.; Friend, R. H.; Brédas, J.-L.; Li, F., High stability and luminescence efficiency in donor–acceptor neutral radicals not following the Aufbau principle. *Nat. Mater.* **2019**, *18* (9), 977-984.
38. Murata, R.; Wang, Z.; Miyazawa, Y.; Antol, I.; Yamago, S.; Abe, M., SOMO–HOMO Conversion in Triplet Carbenes. *Org. Lett.* **2021**, *23* (13), 4955-4959.
39. Murata, R.; Wang, Z.; Abe, M., Singly Occupied Molecular Orbital−Highest Occupied Molecular Orbital (SOMO−HOMO) Conversion. *Aust. J. Chem.* **2021**, *74* (12), 827.
40. Gryn'ova, G.; Coote, M. L.; Corminboeuf, C., Theory and practice of uncommon molecular electronic configurations. *WIREs: Comput. Mol. Sci.* **2015**, *5* (6), 440-459.
41. Abella, L.; Crassous, J.; Favereau, L.; Autschbach, J., Why is the Energy of the Singly Occupied Orbital in Some Radicals below the Highest Occupied Orbital Energy? *Chem. Mater.* **2021**, *33* (10), 3678-3691.
42. Ueda, A.; Wasa, H.; Suzuki, S.; Okada, K.; Sato, K.; Takui, T.; Morita, Y., Chiral Stable Phenalenyl Radical: Synthesis, Electronic-Spin Structure, and Optical Properties of [4]Helicene-Structured Diazaphenalenyl. *Angew. Chem. Int. Ed.* **2012**, *51* (27), 6691-6695.
43. Gliemann, B. D.; Petrovic, A. G.; Zolnhofer, E. M.; Dral, P. O.; Hampel, F.; Breitenbruch, G.; Schulze, P.; Raghavan, V.; Meyer, K.; Polavarapu, P. L.; Berova, N.; Kivala, M., Configurationally Stable Chiral Dithia-Bridged Hetero[4]helicene Radical Cation: Electronic Structure and Absolute Configuration. *Chem. Asian J.* **2017**, *12* (1), 31-35.
44. Ivanov, M. V.; Thakur, K.; Bhatnagar, A.; Rathore, R., Isolation of a chiral anthracene cation radical: X-ray crystallography and computational interrogation of its racemization. *Chem. Commun.* **2017**, *53* (18), 2748-2751.
45. Hsieh, Y. C.; Wu, C. F.; Chen, Y. T.; Fang, C. T.; Wang, C. S.; Li, C. H.; Chen, L. Y.; Cheng, M. J.; Chueh, C. C.; Chou, P. T.; Wu, Y. T., 5,14-Diaryldiindeno[2,1- f:1',2' -j]picene: A New Stable [7]Helicene with a Partial Biradical Character. *J. Am. Chem. Soc.* **2018**, *140* (43), 14357-14366.
46. Inoue, Y.; Sakamaki, D.; Tsutsui, Y.; Gon, M.; Chujo, Y.; Seki, S., Hash-Mark-Shaped Azaacene Tetramers with Axial Chirality. *J. Am. Chem. Soc.* **2018**, *140* (23), 7152-7158.
47. Narita, M.; Teraoka, T.; Murafuji, T.; Shiota, Y.; Yoshizawa, K.; Mori, S.; Uno, H.; Kanegawa, S.; Sato, O.; Goto, K.; Tani, F., An Azulene-Based Chiral Helicene and Its Air-Stable Cation Radical. *Bull. Chem. Soc. Jpn.* **2019**, *92* (11), 1867-1873.
48. Prince, R.; Tomáš, Š.; Michel, R.; Daniel, H.; Markus, N.; Martin, B.; Michal, J., Cethrene: A Helically Chiral Biradicaloid Isomer of Heptazethrene. *Angew. Chem. Int. Ed.* **2016**, *55* (3), 1183-1186.
49. Ravat, P.; Solomek, T.; Haussinger, D.; Blacque, O.; Juricek, M., Dimethylcethrene: A Chiroptical Diradicaloid Photoswitch. *J. Am. Chem. Soc.* **2018**, *140* (34), 10839-10847.
50. Shen, C.; Loas, G.; Srebro-Hooper, M.; Vanthuyne, N.; Toupet, L.; Cador, O.; Paul, F.; Lopez Navarrete, J. T.; Ramirez, F. J.; Nieto-Ortega, B.; Casado, J.; Autschbach, J.; Vallet, M.; Crassous, J., Iron Alkynyl Helicenes: Redox-Triggered Chiroptical Tuning in the IR and Near-IR Spectral Regions and Suitable for Telecommunications Applications. *Angew. Chem. Int. Ed.* **2016**, *55* (28), 8062-8066.
51. Atzori, M.; Dhbaibi, K.; Douib, H.; Grasser, M.; Dorcet, V.; Breslavetz, I.; Paillot, K.; Cador, O.; Rikken, G. L. J. A.; Le Guennic, B.; Crassous, J.; Pointillart, F.; Train, C., Helicene-Based Ligands Enable Strong Magneto-Chiral Dichroism in a Chiral Ytterbium Complex. *J. Am. Chem. Soc.* **2021**, *143* (7), 2671-2675.
52. Atzori, M.; Ludowieg, H. D.; Valentín-Pérez, Á.; Cortijo, M.; Breslavetz, I.; Paillot, K.; Rosa, P.; Train, C.; Autschbach, J.; Hillard, E. A.; Rikken, G. L. J. A., Validation of

microscopic magnetochiral dichroism theory. *Sci. Adv.* **2021**, *7* (17), eabg2859.
53. Mayorga-Burrezo, P.; Jimenez, V. G.; Blasi, D.; Parella, T.; Ratera, I.; Campana, A. G.; Veciana, J., An Enantiopure Propeller-Like Trityl-Brominated Radical: Bringing Together a High Racemization Barrier and an Efficient Circularly Polarized Luminescent Magnetic Emitter. *Chem. Eur. J.* **2020**, *26* (17), 3776-3781.
54. Mayorga Burrezo, P.; Jimenez, V. G.; Blasi, D.; Ratera, I.; Campana, A. G.; Veciana, J., Organic Free Radicals as Circularly Polarized Luminescence Emitters. *Angew. Chem. Int. Ed.* **2019**, *58* (45), 16282-16288.
55. Shil, S.; Bhattacharya, D.; Misra, A.; Klein, D. J., A high-spin organic diradical as a spin filter. *Phys. Chem. Chem. Phys.* **2015**, *17* (36), 23378-23383.
56. Frederic, L.; Desmarchelier, A.; Favereau, L.; Pieters, G., Designs and Applications of Circularly Polarized Thermally Activated Delayed Fluorescence Molecules. *Adv. Funct. Mater.* **2021**, *31* (20), 2010281.
57. Zhang, D. W.; Li, M.; Chen, C. F., Recent advances in circularly polarized electroluminescence based on organic light-emitting diodes. *Chem Soc Rev* **2020**, *49* (5), 1331-1343.
58. Lindemann, M.; Xu, G.; Pusch, T.; Michalzik, R.; Hofmann, M. R.; Žutić, I.; Gerhardt, N. C., Ultrafast spin-lasers. *Nature* **2019**, *568* (7751), 212-215.
59. Sergey, S.; A., F. M.; David, P., Monitoring of the ADP/ATP Ratio by Induced Circularly Polarised Europium Luminescence. *Angew. Chem. Int. Ed.* **2018**, *57* (25), 7488-7492.
60. *i.e*. when the unpaired electron is within the chiral π-conjugated system.
61. Tan, J. S. J.; Paton, R. S., Frontier molecular orbital effects control the hole-catalyzed racemization of atropisomeric biaryls. *Chem. Sci.* **2019**, *10* (8), 2285-2289.
62. Kasemthaveechok, S.; Abella, L.; Jean, M.; Cordier, M.; Roisnel, T.; Vanthuyne, N.; Guizouarn, T.; Cador, O.; Autschbach, J.; Crassous, J.; Favereau, L., Axially and Helically Chiral Cationic Radical Bicarbazoles: SOMO-HOMO Level Inversion and Chirality Impact on the Stability of Mono- and Diradical Cations. *J. Am. Chem. Soc.* **2020**, *142* (48), 20409-20418.
63. Rajca, A.; Shu, C.; Zhang, H.; Zhang, S.; Wang, H.; Rajca, S., Thiophene-Based Double Helices: Radical Cations with SOMO-HOMO Energy Level Inversion. *Photochem. Photobiol.* **2021**, *97* (6), 1376-1390.
64. Mallick, S.; Maddala, S.; Kollimalayan, K.; Venkatakrishnan, P., Oxidative Coupling of Carbazoles: A Substituent-Governed Regioselectivity Profile. *J. Org. Chem.* **2019**, *84* (1), 73-93.
65. Sumsalee, P.; Abella, L.; Roisnel, T.; Lebrequier, S.; Pieters, G.; Autschbach, J.; Crassous, J.; Favereau, L., Axial and helical thermally activated delayed fluorescence bicarbazole emitters: Opposite modulation of circularly polarized luminescence through intramolecular charge-transfer dynamics. *J. Mater. Chem. C* **2021**, *9* (35), 11905-11914.
66. Gingras, M.; Felix, G.; Peresutti, R., One hundred years of helicene chemistry. Part 2: stereoselective syntheses and chiral separations of carbohelicenes. *Chem. Soc. Rev.* **2013**, *42* (3), 1007-1050.
67. C.-F. Chen; Shen, Y., *Helicenes Chemistry: From Synthesis to Applications*. Springer, Berlin: **2017**.
68. Dhbaibi, K.; Favereau, L.; Crassous, J., Enantioenriched Helicenes and Helicenoids Containing Main-Group Elements (B, Si, N, P). *Chem. Rev.* **2019**, *119* (14), 8846-8953.
69. M. J. Frisch, G. W. T., H. B. Schlegel, G. E. Scuseria, ; M. A. Robb, J. R. C., G. Scalmani, V. Barone, ; G. A. Petersson, H. N., X. Li, M. Caricato, A. V. Marenich, ; J. Bloino, B. G. J., R. Gomperts, B. Mennucci, H. P. Hratchian, ; J. V. Ortiz, A. F. I., J. L. Sonnenberg, D. Williams-Young, ; F. Ding, F. L., F. Egidi, J. Goings, B. Peng, A. Petrone, ; T. Henderson, D. R., V. G. Zakrzewski, J. Gao, N. Rega, ; G. Zheng, W. L., M. Hada, M. Ehara, K. Toyota, R. Fukuda, ; J. Hasegawa, M. I., T. Nakajima, Y. Honda, O. Kitao, H. Nakai, ; T. Vreven, K. T., J. A. Montgomery, Jr., J. E. Peralta, ; F. Ogliaro, M. J. B., J. J. Heyd, E. N. Brothers, K. N. Kudin, ; V. N. Staroverov, T. A. K., R. Kobayashi, J. Normand, ; K. Raghavachari, A. P. R., J. C. Burant, S. S. Iyengar, ; J. Tomasi, M. C., J. M. Millam, M. Klene, C. Adamo, R. Cammi, ; J. W. Ochterski, R. L. M., K. Morokuma, O. Farkas, ; J. B. Foresman, D. J. F., "Gaussian 16, Revision B.01". Gaussian, Inc., Wallingford CT: **2016**. URL: www.gaussian.com (accessed 2022-03-21).
70. Adamo, C.; Barone, V., Toward reliable density functional methods without adjustable parameters: The PBE0 model. *J. Chem. Phys.* **1999**, *110* (13), 6158-6170.
71. Weigend, F.; Ahlrichs, R., Balanced basis sets of split valence, triple zeta valence and quadruple zeta valence quality for H to Rn: Design and assessment of accuracy. *Phys. Chem. Chem. Phys.* **2005**, *7* (18), 3297-3305.
72. Weigend, F., Accurate Coulomb-fitting basis sets for H to Rn. *Phys. Chem. Chem. Phys.* **2006**, *8* (9), 1057-1065.
73. Scalmani, G.; Frisch, M. J., Continuous surface charge polarizable continuum models of solvation. I. General formalism. *J. Chem. Phys.* **2010**, *132* (11), 114110.
74. Grimme, S.; Antony, J.; Ehrlich, S.; Krieg, H., A consistent and accurate ab initio parametrization of density functional dispersion correction (DFT-D) for the 94 elements H-Pu. *J. Chem. Phys.* **2010**, *132* (15), 154104.
75. Autschbach, J.; Nitsch-Velasquez, L.; Rudolph, M., Time-dependent density functional response theory for electronic chiroptical properties of chiral molecules. *Top. Curr. Chem.* **2011**, *298*, 1-98.
76. Srebro-Hooper, M.; Autschbach, J., Calculating Natural Optical Activity of Molecules from First Principles. *Annu. Rev. Phys. Chem.* **2017**, *68* (1), 399-420.
77. Chiu, S. K.; Chung, Y. C.; Liou, G. S.; Su, Y. O., Electrochemical and Spectral Characterizations of 9-Phenylcarbazoles. *Jnl. Chinese Chemical Soc.* **2012**, *59* (3), 331-337.
78. Karon, K.; Lapkowski, M., Carbazole electrochemistry: a short review. *J. Solid State Chem.* **2015**, *19* (9), 2601-2610.
79. Connelly, N. G.; Geiger, W. E., Chemical Redox Agents for Organometallic Chemistry. *Chem. Rev.* **1996**, *96* (2), 877-910.
80. Kusamoto, T.; Kume, S.; Nishihara, H., Realization of SOMO−HOMO Level Conversion for a TEMPO-Dithiolate Ligand by Coordination to Platinum(II). *J. Am. Chem. Soc.* **2008**, *130* (42), 13844-13845.
81. Ratera, I.; Veciana, J., Playing with organic radicals as building blocks for functional molecular materials. *Chem. Soc. Rev.* **2012**, *41* (1), 303-349.
82. Banerjee-Ghosh, K.; Ben Dor, O.; Tassinari, F.; Capua, E.; Yochelis, S.; Capua, A.; Yang, S.-H.; Parkin, S. S. P.; Sarkar, S.; Kronik, L.; Baczewski, L. T.; Naaman, R.; Paltiel, Y., Separation of enantiomers by their enantiospecific interaction with achiral magnetic substrates. *Science* **2018**, *360* (6395), 1331-1334.
83. Naaman, R.; Paltiel, Y.; Waldeck, D. H., Chiral molecules and the electron spin. *Nat. Rev. Chem.* **2019**, *3* (4), 250-260.
84. Naaman, R.; Paltiel, Y.; Waldeck, D. H., Chiral Molecules and the Spin Selectivity Effect. *J. Phys. Chem. Lett.* **2020**, *11* (9), 3660-3666.
85. Kim, Y.-H.; Zhai, Y.; Lu, H.; Pan, X.; Xiao, C.; Gaulding, E. A.; Harvey, S. P.; Berry, J. J.; Vardeny, Z. V.; Luther, J. M.; Beard, M. C., Chiral-induced spin selectivity enables a room-temperature spin light-emitting diode. *Science* **2021**, *371* (6534), 1129-1133.

86. Hankache, J.; Wenger, O. S., Organic Mixed Valence. *Chem. Rev.* **2011**, *111* (8), 5138-5178.
87. Heckmann, A.; Lambert, C., Organic Mixed-Valence Compounds: A Playground for Electrons and Holes. *Angew. Chem. Int. Ed.* **2012**, *51* (2), 326-392.
88. Lambert, C.; Nöll, G., The Class II/III Transition in Triarylamine Redox Systems. *J. Am. Chem. Soc.* **1999**, *121* (37), 8434-8442.
89. Nakazaki, J.; Matsushita, M. M.; Izuoka, A.; Sugawara, T., Novel spin-polarized TTF donors affording ground state triplet cation diradicals. *Tetrahedron Lett.* **1999**, *40* (27), 5027-5030.
90. Eaton, S. S.; More, K. M.; Sawant, B. M.; Eaton, G. R., Use of the ESR half-field transition to determine the interspin distance and the orientation of the interspin vector in systems with two unpaired electrons. *J. Am. Chem. Soc.* **1983**, *105* (22), 6560-6567.
91. Bleaney, B.; Bowers, K. D., Anomalous paramagnetism of copper acetate. *Proceedings of the Royal Society of London. Series A. Mathematical and Physical Sciences* **1952**, *214* (1119), 451-465.
92. Borden, W. T.; Davidson, E. R., Effects of electron repulsion in conjugated hydrocarbon diradicals. *J. Am. Chem. Soc.* **1977**, *99* (14), 4587-4594.
93. Malrieu, J. P.; Caballol, R.; Calzado, C. J.; de Graaf, C.; Guihéry, N., Magnetic Interactions in Molecules and Highly Correlated Materials: Physical Content, Analytical Derivation, and Rigorous Extraction of Magnetic Hamiltonians. *Chem. Rev.* **2014**, *114* (1), 429-492.
94. Wang, Z.; Murata, R.; Abe, M., SOMO-HOMO Conversion in Triplet Cyclopentane-1,3-diyl Diradicals. *ACS Omega* **2021**, *6* (35), 22773-22779.
95. Center for Computational Research, University at Buffalo, http://hdl.handle.net/10477/79221 (accessed 2022-03-21).

Insert Table of Contents artwork here